

Simplifying multi-level thermal machines using virtual qubits

Ayaka Usui,^{1,*} Wolfgang Niedenzu,^{2,†} and Marcus Huber^{3,‡}

¹*Quantum Systems Unit, Okinawa Institute of Science and Technology Graduate University, Onna, Okinawa 904-0495, Japan*

²*Institut für Theoretische Physik, Universität Innsbruck, Technikerstraße 21a, A-6020 Innsbruck, Austria*

³*Institute for Quantum Optics and Quantum Information - IQOQI Vienna,
Austrian Academy of Sciences, Boltzmannngasse 3, 1090 Vienna, Austria*

(Dated: April 25, 2022)

Quantum thermodynamics often deals with the dynamics of small quantum machines interfacing with a large and complex environment. Virtual qubits, collisional models and reset master equations have become highly useful tools for predicting the qualitative behaviour of two-dimensional target systems coupled to few qubit machines and a thermal environment. While matching the simplified model parameters for all possible physical systems is an impossibly hard task in general, the qualitative predictions still allow for a general design of quantum machines irrespective of the implementation. We generalise these tools by introducing multiple competing virtual qubits for modelling multi-dimensional systems coupled to larger and more complex machines. By simulating the full physical dynamics for targets with three dimensions, we uncover general properties of reset models that can be used as ‘dials’ to correctly predict the qualitative features of physical changes in a realistic setup and thus design autonomous quantum machines beyond a few qubits. We then present a general analytic solution of the reset model for arbitrary-dimensional systems coupled to multi-qubit machines. Finally, we showcase an improved three-level laser as an exemplary application of our results.

I. INTRODUCTION

Machines operating at the quantum scale offer an exploration of the ultimate limits of thermodynamic tasks [1–8], such as cooling down individual quantum systems or creating coherent sources of light. Design and control of such processes is usually assumed an achieved at the level of few quantum mechanical degrees of freedom, interacting with a large environment that one lacks detailed control over [9–14]. As large quantum systems are notoriously hard to simulate exactly, most of the focus is devoted on deriving master equations and dynamics for few-qubit machines or a single qutrit interacting with multiple baths. A crucial discovery in that context is the concept of a virtual qubit [15–17]. It allows to predict the steady state and even transient dynamics of a two level transition of interest by focusing on the two levels that the transition effectively interacts with, which is called a virtual qubit. It dramatically reduces the complexity of predicting relevant machine behaviour, by sacrificing detailed knowledge of how the complex machine creating the virtual qubit behaves and shifts focus only on the target system of interest [18–21]. Going beyond simple qubit targets, however, is a challenge due to the potential complexity of competing interactions with multiple virtual qubits. In this paper, we solve the problem, for arbitrary-dimensional quantum systems (qudits), interacting with multiple competing virtual qubits across all possible two-level transitions in the context of reset-type master equations. We explore the solution for three-level

quantum systems and compare it to optical master equations, identifying a few universal features that these approaches share and thus important properties of complex machine designs that this simple and computable model correctly predicts. Finally, we use our model and analysis to study an enhancement of the paradigmatic three-level maser/laser [22] through more complex machines.

II. MOTIVATION: THE TWO-QUBIT MACHINE AS A VIRTUAL QUBIT

First, we review the idea of virtual qubits, which has been proposed in Ref. [15]. Consider two qubits with energy spacings Ω_1 and Ω_2 (we assume $\Omega_1 > \Omega_2$) that are in contact with two thermal baths at temperatures T_1 and T_2 , respectively. This two-qubit machine is composed of the energy eigenstates $|0\rangle_1|0\rangle_2$, $|0\rangle_1|1\rangle_2$, $|1\rangle_1|0\rangle_2$, and $|1\rangle_1|1\rangle_2$. The single-excitation manifold is then called a *virtual qubit* whose ground and excited state are given by $|0\rangle_1|1\rangle_2$ and $|1\rangle_1|0\rangle_2$, respectively, with the energy spacing $\Omega_1 - \Omega_2$. The temperature of this virtual qubit, called the virtual temperature, is determined by the ratio between of the ground- and excited state populations, which, together with the Boltzmann law, leads to

$$T_v = \frac{\Omega_1 - \Omega_2}{\Omega_1/T_1 - \Omega_2/T_2}. \quad (1)$$

Note that, since it is not a real temperature, T_v may be negative in the case of population inversion.

We now add another physical qubit, namely the *target qubit*, with energy spacing $\omega_1 - \omega_0 = \Omega_1 - \Omega_2$ that is coherently coupled to the two-qubit machine (see Fig. 1). Assuming that this target qubit is further interacting with an environment at temperature T_{en} , the dynam-

* ayaka.usui@oist.jp

† Wolfgang.Niedenzu@uibk.ac.at

‡ marcus.huber@univie.ac.at

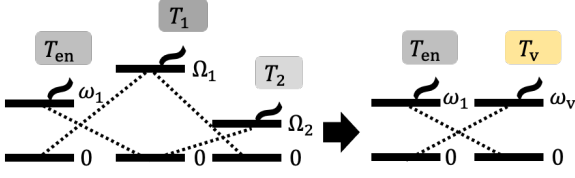


Figure 1. Sketch of a virtual qubit. Left: a target qubit coupled to a two-qubit machine, where $\omega_1 - \omega_0 = \Omega_1 - \Omega_2$ and $\omega_0 = 0$. Right: the target qubit effectively coupled to a virtual qubit, where $\omega_v = \Omega_1 - \Omega_2$ and T_v is given by Eq. (1). The dotted lines represent coherent interaction given in Eq. (3).

ics of the composite system are determined by the reset master equation (RME) [16]

$$\begin{aligned} \frac{\partial \rho_{\text{tot}}}{\partial t} = & -i[H, \rho_{\text{tot}}] + Q_{\text{en}} (\tau_{\text{en}} \otimes \text{Tr}_{\text{tar}}[\rho_{\text{tot}}] - \rho_{\text{tot}}) \\ & + Q_1 (\tau_1 \otimes \text{Tr}_1[\rho_{\text{tot}}] - \rho_{\text{tot}}) \\ & + Q_2 (\tau_2 \otimes \text{Tr}_2[\rho_{\text{tot}}] - \rho_{\text{tot}}), \end{aligned} \quad (2)$$

where ρ_{tot} is the density matrix of the composite system. Here, $Q_{\text{en},1,2}$ are thermalisation rates corresponding to the environment or the thermal baths in contact with the two-qubit machine, respectively. The density matrices $\tau_{\text{en},1,2}$ are thermal states corresponding to the real temperatures T_{en}, T_1 and T_2 , respectively. The partial traces over the target qubit or the machine's constituents are denoted $\text{Tr}_{\text{tar},1,2}$, respectively. The Hamiltonian in Eq. (2) reads

$$H = \sum_{k=0}^1 \omega_k |k\rangle\langle k| + \sum_{i \in \{1,2\}} \Omega_i \sigma_i^+ \sigma_i^- + g |0\rangle\langle 1| \sigma_1^+ \sigma_2^- + \text{H.c.} \quad (3)$$

with $\sigma_i^+ = |1\rangle_i \langle 0|_i$ and the coherent coupling strength g . Without the environment, the dynamics drive the target qubit into a steady state at the virtual temperature (1) [16], independent of the rates Q_1 and Q_2 .

In general, however, the two-qubit machine is disturbed by the target qubit's interaction with the environment and hence the virtual temperature (1) is not the steady state temperature anymore. However, if the qubits inside the two-qubit machine thermalise very fast with the two baths at temperatures $T_{1,2}$, i.e., if $Q_{1,2} \gg Q_{\text{en}}, g$, the notion of the virtual temperature (1) remains valid.

Here, assuming $Q_{1,2} \gg Q_{\text{en}}, g$, we replace the two-qubit machine with a bath at the virtual temperature (1) and consider the effective reset master equation (effRME) for the target system only,

$$\frac{\partial \rho}{\partial t} = Q_{\text{en}} (\tau_{\text{en}} - \rho) + q_{\text{vir}} (\tau_{\text{vir}} - \rho), \quad (4)$$

where q_{vir} is the effective thermalisation rate to the virtual qubit and τ_{vir} is a thermal state at the virtual temperature (1).

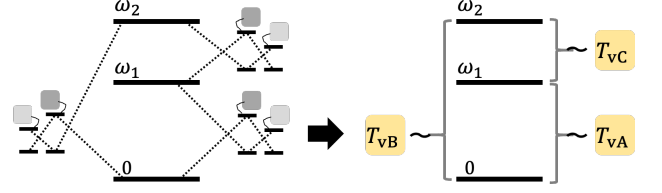


Figure 2. Simplification of two-qubit machines by using virtual qubits, where $\omega_0 = 0$. Left: a qutrit coupled with three two-qubit machines. The dotted lines represent coherent interaction. Right: the qutrit where all the two-qubit machines are assumed to be baths at the virtual temperatures.

The steady-state solution of this effective reset master equation reads

$$\rho_{\text{ss}} = C (Q_{\text{en}} \tau_{\text{en}} + q_{\text{vir}} \tau_{\text{vir}}) \quad (5)$$

with the normalisation $C = (Q_{\text{en}} + q_{\text{vir}})^{-1}$. Note that owing to the two competitive dissipative couplings, this steady-state solution explicitly depends on the rates Q_{en} and q_{vir} .

Comparing this steady state (5) of the effRME with that from the RME (2), and using $Q_{1,2} \gg q_{\text{en}}, g$, we find

$$q_{\text{vir}} = \frac{2g^2}{Q_1 + Q_2} (\tau_1^g \tau_2^e + \tau_1^e \tau_2^g). \quad (6)$$

Here, $\tau_{1,2}^{g,e}$ are the populations of the ground and excited states of the thermal state at temperatures $T_{1,2}$, respectively. We therefore denote

$$n_{\text{vir}} = \tau_1^g \tau_2^e + \tau_1^e \tau_2^g \quad (7)$$

the *norm* of the virtual qubit, as it corresponds to the weight of the levels $|0\rangle_1 |1\rangle_2$ and $|1\rangle_1 |0\rangle_2$ that form the virtual qubit within the two-qubit machine space. This norm thus determines the temperature dependence of the effective rate q_{vir} .

III. THREE-LEVEL SYSTEM COUPLED TO THREE TWO-LEVEL MACHINES

We now continue by applying the idea of virtual qubits to higher-dimensional target systems. In this section, we consider a three-level system, i.e., a qutrit, with energy spacings $\omega_{0,1,2}$ that is

coupled to several two-qubit machines (Fig. 2). Within the effRME description, each of these two-qubit machines is regarded as a virtual qubit.

With a single machine coupled to the target qutrit, the situation is essentially the same as the qubit target shown Fig. 1. With two machines coupled, two distinct thermalisation processes act on the target. Consequently, the steady state of the latter is not a Gibbs-like state, unless both virtual temperatures are the same. As an example, if a machine with virtual temperature T_{v1} is

connected to the target levels $|0\rangle$ and $|1\rangle$ and another one with virtual temperature T_{v2} is connected to the levels of $|0\rangle$ and $|2\rangle$, the qutrit is driven into the steady state

$$\rho_{ss} = C \left(|0\rangle\langle 0| + e^{-(\omega_1 - \omega_0)/T_{v1}} |1\rangle\langle 1| + e^{-(\omega_2 - \omega_0)/T_{v2}} |2\rangle\langle 2| \right) \quad (8)$$

with the normalisation $C = (1 + e^{-(\omega_1 - \omega_0)/T_{v1}} + e^{-(\omega_2 - \omega_0)/T_{v2}})^{-1}$. As the two thermalisation processes do not compete, each transition is “thermalised” to its respective virtual temperature T_{v1}, T_{v2} .

By contrast, if all transitions within the target qutrit interact with independent two-level machines (Fig. 2), the three thermalisation processes compete against each other unless all the virtual temperatures are equal.

In the following, we utilise the idea of the virtual qubits to construct an effective reset master equation of the three-level target system as we did for the qubit target system. To explore the parameter dependency of the effective thermalisation rates, we compare the steady state among the effective reset master equation (effRME) for the target system, the full reset master equation (RME) for target plus machine, and the GKLS master equation (GKLSME) as non-exclusive physical models for the corresponding machine setup. Finally, we discuss these models’ relations to the effRME.

III.1. Effective reset master equation (effRME)

We consider a qutrit coherently coupled to three pairs of two physical qubits, as depicted in Fig. 2. We label as “A” the pair coupled to the levels of $|0\rangle$ and $|1\rangle$, as “B” the pair coupled to the levels of $|0\rangle$ and $|2\rangle$, and as “C” the pair coupled to the levels of $|1\rangle$ and $|2\rangle$. Each of the pairs has two qubits with energy spacings Ω_{i1} and Ω_{i2} , and the qubits are in contact to baths of which temperatures are T_{i1} and T_{i2} , respectively, for $i \in \{A, B, C\}$. Furthermore, due to energy conservation, the energy spacings are restricted as $\omega_1 - \omega_0 = \Omega_{A1} - \Omega_{A2}$, $\omega_2 - \omega_0 = \Omega_{B1} - \Omega_{B2}$, and $\omega_2 - \omega_1 = \Omega_{C1} - \Omega_{C2}$.

We assume that the thermalisation in the qubits inside the two-qubit machines to the baths is fast enough that the virtual temperatures are valid. By considering that the two-qubit machines maintain their virtual temperatures, the effective reset master equation of the target system (effRME) is provided by

$$\frac{\partial \rho}{\partial t} = \sum_{i \in \{A, B, C\}} q_i (\tau_i \otimes \text{Tr}_i[\rho] - \rho), \quad (9)$$

where $q_{A,B,C}$ is the effective thermalisation rate and $\text{Tr}_{A,B,C}$ represents tracing out the space of the qubit pair A, B, C. The states $\tau_{A,B,C}$ are thermal state at the virtual temperatures T_{vA}, T_{vB}, T_{vC} given by

$$T_{vi} = \frac{\Omega_{i1} - \Omega_{i2}}{\Omega_{i1}/T_{i1} - \Omega_{i2}/T_{i2}} \quad (10)$$

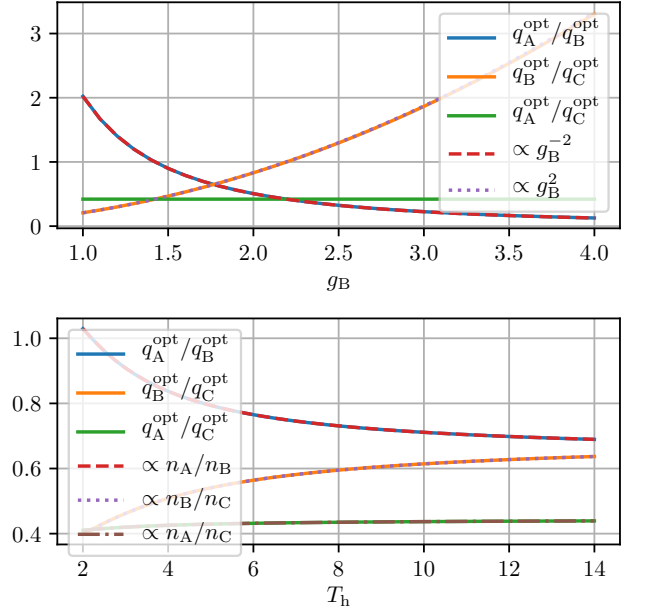


Figure 3. Optimal Hamiltonian coupling coefficients between the target qutrit and the auxiliary qubits for which the state (11) is the steady-state solution of the RME (13) as a function of coherent interaction strength g_B (upper panel) and bath temperature $T_{i1} = T_h$ (lower panel). The both plots use the same parameter set, except for $T_{i1} = T_h = 3.1$ in the upper panel and $g_B = 1.5$ in the lower panel. Apart from the two parameters, the following is used: $\omega_0 = 0$, $\omega_1 = 2$, $\omega_2 = 3$, $\Omega_{A1} = 2.5$, $\Omega_{B1} = 4.5$, $\Omega_{C1} = 1.3$, $g_A = 1.2$, $g_C = 1.8$, $T_{i1} = T_h = 3.1$, $T_{i2} = T_c = 1.2$, $Q_{i1} = 70$, and $Q_{i2} = 50$ for $i \in \{A, B, C\}$. In the upper panel, the ratio q_A/q_B is proportional to $1/g_B^2$, and the ratio q_B/q_C is proportional to g_B^2 . In the lower panel, the ratios q_i/q_j are proportional to the ratios n_i/n_j of the norms (15) of the virtual qubits for $i, j \in \{A, B, C\}$

for $i \in \{A, B, C\}$. Explicitly, these states read $\tau_A = \tau_A^g |0\rangle\langle 0| + \tau_A^e |1\rangle\langle 1|$, $\tau_B = \tau_B^g |0\rangle\langle 0| + \tau_B^e |2\rangle\langle 2|$, and $\tau_C = \tau_C^g |1\rangle\langle 1| + \tau_C^e |2\rangle\langle 2|$, respectively, where $\tau_i^{g,e}$ are the respective populations of the ground and excited states. By solving the effRME (9) for $\partial \rho / \partial t = 0$, the steady state of the target system is obtained as

$$\rho_{ss} = C (q_A q_B \tau_{AB} + q_B q_C \tau_{BC} + q_C q_A \tau_{CA}), \quad (11)$$

where the normalisation is $C = (q_A q_B \text{Tr}[\tau_{AB}] + q_B q_C \text{Tr}[\tau_{BC}] + q_C q_A \text{Tr}[\tau_{CA}])^{-1}$. The steady state (11) of the target system is thus a combination of the respective steady states if only two of the three coherent couplings are present, i.e.,

$$\tau_{AB} = \tau_A^g \tau_B^g |0\rangle\langle 0| + \tau_A^e \tau_B^g |1\rangle\langle 1| + \tau_A^g \tau_B^e |2\rangle\langle 2|, \quad (12a)$$

$$\tau_{BC} = \tau_B^g \tau_C^g |0\rangle\langle 0| + \tau_B^e \tau_C^g |1\rangle\langle 1| + \tau_B^g \tau_C^e |2\rangle\langle 2|, \quad (12b)$$

$$\tau_{CA} = \tau_C^g \tau_A^g |0\rangle\langle 0| + \tau_C^e \tau_A^g |1\rangle\langle 1| + \tau_C^g \tau_A^e |2\rangle\langle 2|. \quad (12c)$$

Note that these states are not normalised on purpose, i.e., $\text{Tr}[\tau_{AB}] \neq 1$, $\text{Tr}[\tau_{BC}] \neq 1$, and $\text{Tr}[\tau_{CA}] \neq 1$.

We have generalised this virtual-qubit treatment to

higher-dimensional target systems, see Appendices A and B.

III.2. Reset master equation (RME)

Here, we present the reset master equation (REM) for the composite system (target and machine) and compare its steady state with the steady state (11) of the effRME.

The RME describing the composite system reads

$$\frac{\partial \rho_{\text{tot}}}{\partial t} = -i[H, \rho_{\text{tot}}] + \sum_{i \in \mathcal{I}} Q_i (\tau_i \otimes \text{Tr}_i[\rho_{\text{tot}}] - \rho_{\text{tot}}), \quad (13)$$

with the respective thermalisation rates Q_i for $\mathcal{I} := \{A1, A2, B1, B2, C1, C2\}$ and the Hamiltonian

$$H = \sum_{k=0}^2 \omega_k |k\rangle\langle k| + \sum_{i \in \mathcal{I}} \Omega_i \sigma_i^+ \sigma_i^- + [g_A |0\rangle\langle 1| \sigma_{A1}^+ \sigma_{A2}^- + g_B |0\rangle\langle 2| \sigma_{B1}^+ \sigma_{B2}^- + g_C |1\rangle\langle 2| \sigma_{C1}^+ \sigma_{C2}^- + \text{H.c.}] \quad (14)$$

with the coupling strengths $g_{A,B,C}$ to each of the subsystems and the qubit frequencies $\Omega_{A2} := \Omega_{A1} - (\omega_1 - \omega_0)$, $\Omega_{B2} := \Omega_{B1} - (\omega_2 - \omega_0)$, $\Omega_{C2} := \Omega_{C1} - (\omega_2 - \omega_1)$. While the solution of $\partial \rho_{\text{tot}} / \partial t = 0$ provides the steady state of the composite system, solving this equation analytically is difficult due to the size of the system, which is $3 \times 2^2 \times 2^2 \times 2^2 = 192$. Even if numerical solutions of $\partial \rho_{\text{tot}} / \partial t = 0$ are obtained, it is hard to understand what the steady state shows physically and what kind of parameters characterise the steady state. Therefore, the effRME is a useful tool.

In order to find the effective thermalisation rates $q_{A,B,C}$ in the effRME, we compute the steady-state solution of the RME (13) in a regime where the thermalisation rates $\{Q_i\}$ are much larger than any other energy scales such that the virtual temperatures are still valid and compare it to the solution (11) of the effRME.

Assuming that all the two-qubit machines are subject to the same bath temperatures, i.e., $T_{i1} = T_h$ and $T_{i2} = T_c$ for $i \in \{A, B, C\}$, we plot the ratio of the effective thermalisation rates $q_{A,B,C}$ as a function of the coherent coupling strength $g_{A,B,C}$ and the hot bath temperature T_h in Fig. 3. It is seen that the ratio q_i/q_j is proportional to g_i^2/g_j^2 for $i, j \in \{A, B, C\}$. Further, the T_h -dependency of the ratio q_i/q_j corresponds to the norm of virtual qubits, which, in analogy to Eq. (7), reads

$$n_i = \tau_{i1}^g \tau_{i2}^c + \tau_{i1}^c \tau_{i2}^g \quad (15)$$

for $i \in \{A, B, C\}$. These parameter dependencies are consistent with the effective thermalisation rate (6) in the case of a two-dimensional target system.

III.3. Gorini-Kossakowski-Lindblad-Sudarshan master equation (GKLSME)

We now continue to focus on the case of the target system being a qutrit. The idea of virtual qubits is then to

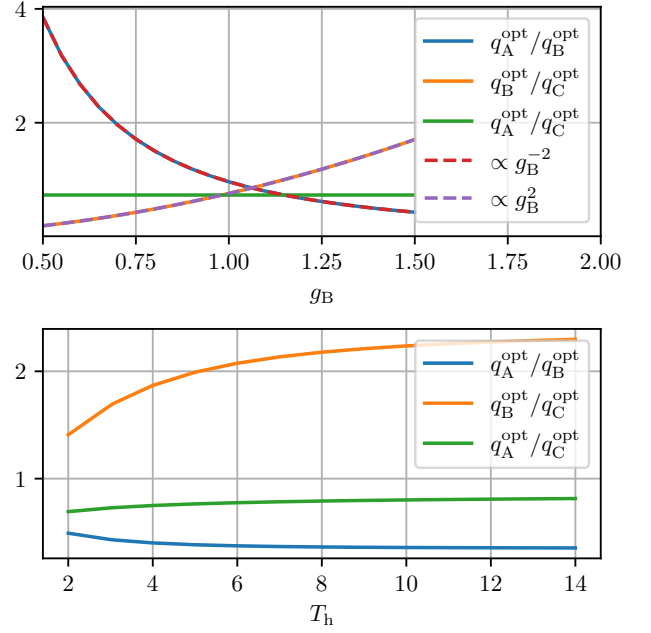


Figure 4. Optimal rates of the effRME (9) for which the state (11) is the steady-state solution of the GKLSME (16) as a function of the coherent coupling strength g_B (upper panel) and the hot-bath temperature T_h (lower panel). The quadratic relation (18) can clearly be seen in the upper panel. Parameters: $T_h = 3.1$ (upper panel) and $g_B = 1.5$ (lower panel). The other parameters are $\omega_0 = 0$, $\omega_1 = 2$, $\omega_2 = 3$, $g_A = 1.2$, $g_C = 1.8$, $\Omega_{A1} = 2.5$, $\Omega_{B1} = 4.5$, $\Omega_{C1} = 1.3$, $T_c = 1.2$, $\Gamma_i = 50$ for $i \in \{A2, B2, C2\}$ and $\Gamma_i = 70$ for $i \in \{A1, B1, C1\}$, respectively, and $t = 10$ (in arbitrary energy units).

replace the “full” RME (13) that governs the dynamics of the joint system composed of the target qutrit and the six physical qubits (with the coupling rates Q_i) by an effRME that contains fewer “virtual” qubits (with the rates q_i). Namely, Eq. (13) is replaced by Eq. (9). The mapping of the rates, $\{Q_i\} \mapsto \{q_i\}$, is, in general, intricate. Notwithstanding, for the case of a target qubit we found the analytic relation (6) whose general features, such as the dependence on the coherent Hamiltonian coupling g_i or the dependence on the norms, could be numerically reproduced for a target qutrit in the foregoing section.

The description of the physical system that underlies the effRME (9) is not unique and may depend on the concrete physical setup. In a sense, the RME (13) constitutes, by itself, also an ad-hoc model. Owing to its CPTP (completely positive and trace-preserving) behaviour, the RME may be cast into a so-called Gorini-Kossakowski-Lindblad-Sudarshan master equation (GKLSME), known from conventional thermalisation models [23–25]. This mapping is, in general, a complicated function of the physical parameters, such as the bath temperatures, and has been explicitly derived for special cases [26]. There, it was shown that in order to fulfil the mapping, the spontaneous emission rates

Γ_i in the GKLSME (see below) must be temperature-dependent, a feature that is usually not encountered in GKLSMEs [25].

On the other hand, we may have also chosen to formulate the original system in terms of a GKLSME with independent rates Γ_i and then map it onto a “full” RME. Thereby, the rates Q_i of the latter become themselves functions of the system parameters. As a consequence, the temperature dependence of the effective rates q_i in the effRME for the target only is expected to depend on more than just the norms of the virtual qubits. The question of which description is more favourable depends on what parameters are easily tunable in a concrete experimental scenario. We will come back to this distinction in the next section and here assume the GKLSME to be the original equation and strive to understand the behaviour of q_i in dependence of the physical parameters.

The GKLSME for a target qutrit that interacts with six physical qubits reads

$$\dot{\rho}_{\text{tot}} = \frac{1}{i}[H, \rho_{\text{tot}}] + \sum_{i \in \mathcal{I}} \mathcal{L}_i \rho_{\text{tot}}, \quad (16)$$

with the Hamiltonian (14) and the qubits $\mathcal{I} = \{A1, A2, B1, B2, C1, C2\}$.

The Liouvillian

$$\mathcal{L}_i \rho = \Gamma_i (\bar{n}(\Omega_i, T_i) + 1) \mathcal{D}[\sigma_i^-] + \Gamma_i \bar{n}(\Omega_i, T_i) \mathcal{D}[\sigma_i^+] \quad (17)$$

describes the dissipative interaction of the i th auxiliary qubit with its bath (see also Fig. 1) at temperature $T_i = T_h$ for $i \in \{A1, B1, C1\}$ and $T_i = T_c$ for $i \in \{A2, B2, C2\}$, respectively; Γ_i is that qubit’s spontaneous emission rate. We have further defined the thermal population $\bar{n}(\omega, T) := [\exp(\omega/T) - 1]^{-1}$ of the bosonic bath and the dissipator $D[A] := 2A\rho A^\dagger - A^\dagger A\rho - \rho A^\dagger A$.

We now replace this equation with the simple effRME (9) for the qutrit only and pose the question: How are the parameters $\{q_A, q_B, q_C\}$ of the effRME (9) related to the parameters of the GKLSME (16)? To answer this question, we numerically integrate the GKLSME (16) for given parameters with the analytic steady-state solution (11), which is parameterised by the triple (q_A, q_B, q_C) , as the initial state of the target qutrit (the qubits were initialised to their respective thermal states). We repeat this integration for different such triples to minimise the Frobenius norm $\|\rho(t) - \rho(0)\|$ between the reduced density operators of the qutrit at time t and time $t = 0$ for a sufficiently large fixed time $t > 0$. The Frobenius norm thus quantifies the deviation of the time-evolved state to the initial state (11). Thereby, we find the optimal parameter triple $(q_A^{\text{opt}}, q_B^{\text{opt}}, q_C^{\text{opt}})$ for which Eq. (11) is the steady-state solution of Eq. (16). By repeating this procedure for, e.g., different T_h , we can then numerically find the dependence of the rates q_i on the physical parameters of the GKLSME (Fig. 4).

As seen from the upper panel in Fig. 4, the quadratic

relation

$$\frac{q_i^{\text{opt}}}{q_j^{\text{opt}}} \propto \frac{g_i^2}{g_j^2} \text{ for } i, j \in \{A, B, C\} \quad (18)$$

of the effective rates in the effRME (9) to the Hamiltonian couplings in the GKLSME (16), first obtained in Eq. (6) for the qubit case, is reproduced, but with different proportionality factors than in Fig. 3. Whilst we only show the dependence on g_B in Fig. 4, we have performed additional simulations for varying g_A and g_C , respectively, that are fully consistent with the quadratic behaviour in Eq. (18).

We have implemented these simulations with the QuantumOptics.jl [27] Julia framework and used Optim.jl [28] for the numerical optimisation procedure.

III.4. Discussion and identifying the “dials”

Our setup possesses a plethora of parameters and the question on how they influence the steady-state solution of the target qutrit is not trivial. What we have seen above is that the behaviour of the optimal q_i^{opt} as a function of, e.g., the hot-bath temperature T_h differs, depending on the description: Whereas in the case of the reset model, the ratios of the q_i^{opt} depend on the corresponding ratio of the norms (15) of the virtual qubits, this is not the case in the GKLS treatment.

To understand this issue it is important to note that in the RME for the seven-body system (target qutrit and six qubits) the parameters Q_i were assumed to be *independent* of the temperature. Therefore, the only temperature dependence in the q_i^{opt} stems from the norm. The GKLSME equivalent to the RME possesses temperature-dependent spontaneous emission rates. By contrast, in Sec. III.3 we have considered rates that do not depend on the temperatures. Therefore, the temperature dependence in Figs. 3 and 4 differ.

It is important to note that although the reset master equation can be written in GKLS form, the latter will not depict the behaviour that we are accustomed to from typical quantum-optical situations: Usually, the decay rates Γ_i do not depend on the temperatures [25], but the rates in the GKLS form of the reset equation will do, similar to Ref. [26]. Therefore, features such as the temperature difference of the steady-state solution strongly depend on whether the Q_i or the Γ_i are assumed to be “auxiliary” parameters with no further dependence on the temperatures. If the Q_i are deemed to be independent, then the Γ_i will depend on the temperatures and, conversely, if the Γ_i are chosen to be independent, then the Q_i will depict a temperature dependence and the lower panel in Fig. 3 would not correspond to the ratio of the norms any more. We note that although the Γ_i in the GKLS description typically depend on the frequencies [25], we may still see them as independent parameters since the frequency dependence may be countered by, e.g., changing the dipole

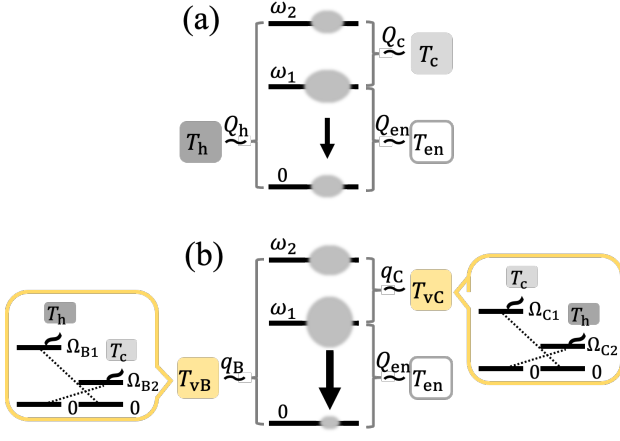


Figure 5. Sketches of (a) a typical laser mechanism with T_h the hot-bath temperature and T_c the cold-bath temperature, and (b) our proposed scheme improved by virtual temperatures, where T_{vB} [Eq. (19)] is negative and T_{vC} [Eq. (20)] is smaller than T_c . The oval on each qutrit level represents this level's population. The lasing transition is further coupled to an environment at temperature T_{en} .

moment of the qubit. It is therefore sensible to assume the rates to be “auxiliary” parameters in either description (although the concrete parameter dependence of the ad-hoc Q_i may be unknown). By contrast, the features that only depend on the Hamiltonian part of the master equation coincide in both descriptions, cf. the quadratic dependence on g_B in Figs. 3 and 4 (the proportionality factors, however, differ).

It is therefore of paramount importance to distinguish between the two genuinely different models

- Reset master equation (RME) with “free” Q_i
- GKLS master equation (GKLSME) with “free” Γ_i

and the mapping of the RME to a GKLSME and vice versa, where the “free” character of the rates no longer holds. The “dials” therefore very much depend on the initial description of the machine, i.e., whether the Q_i or the Γ_i are supposed to be tunable by some auxiliary parameters. Both physical models, RME and GKLSME, therefore have their respective merit in different (experimental) setups.

IV. EXAMPLE: IMPROVING A LASER WITH POPULATION INVERSION

As an exemplary application of our method, we propose a scheme to enhance the output of a three-level laser by coupling it to a complex machine. A typical lasing mechanism [22, 29, 30] is shown in Fig. 5(a). The laser is composed of a three-level system in contact with a hot bath at temperature T_h and a cold bath at T_c that above the lasing threshold creates a population inversion

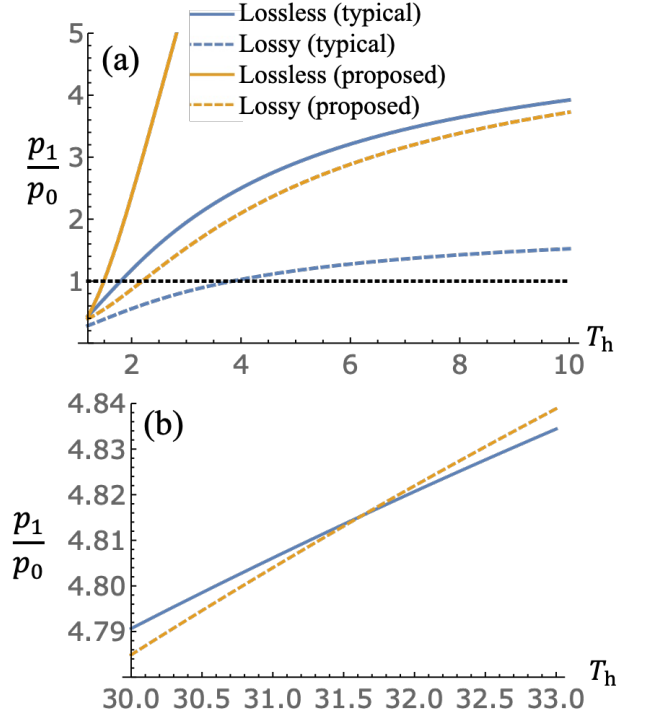


Figure 6. Population ratio p_1/p_0 of the levels $|1\rangle$ and $|0\rangle$ of the qutrit in the typical laser and in our scheme in changing the hot temperature T_h . In (a), the population ratio p_1/p_0 is displayed in cases of the typical laser (directly coupled to the heat baths) and our proposed scheme (indirectly coupled to the baths via two-qubit machines that give rise to virtual temperatures) with (dashed) and without (solid) photon loss. The dotted black line represents the lasing threshold $p_1/p_0 = 1$. “Lossless” (“Lossy”) means no (non-zero) photon loss. The figure (b) zooms in on a regime that our proposed scheme with photon loss considered outperforms the lossless typical laser. The bath temperature and the thermalisation rate associated with loss of the laser output is assumed to be $T_{en} = 7.2$ and $Q_{en} = 2$. For the actual thermalisation rates, $Q_h = 2$, $Q_c = 1.5$, and $Q_{en} = 0.1$ are taken. The other parameters are the same as Figs. 3 and 4: $\omega_0 = 0$, $\omega_1 = 2$, $\omega_2 = 3$, $\Omega_{B1} = 4.5$, $\Omega_{C1} = 1.3$, $T_c = 1.2$.

between the lasing levels $|0\rangle$ and $|1\rangle$. In the following we pose the question: Can this population inversion be increased by indirectly coupling this three-level system to those temperatures via auxiliary two-qubit machines [Fig. 5(b)]?

Namely, we replace the hot bath with a two-qubit machine whose virtual temperature T_{vB} is [cf. Eq. (10)]

$$T_{vB} = \frac{\Omega_{B1} - \Omega_{B2}}{\Omega_{B1}/T_h - \Omega_{B2}/T_c}, \quad (19)$$

where $\Omega_{B2} = \Omega_{B1} - (\omega_2 - \omega_0)$. Note that for a fair comparison, the hot- and cold-bath temperatures used for the laser are also applied to this two-qubit machine. For $T_h > (\Omega_{B1}/\Omega_{B2})T_c$, the virtual temperature T_{vB} is negative and leads to

population inversion between the levels $|2\rangle$ than $|0\rangle$ (see Fig. 5(b)).

Larger population in a higher energy state than a lower energy state is never seen with real thermal baths, but two qubits suffice to generate such an inversion from realistic finite-temperature baths. This population inversion between the levels $|0\rangle$ and $|2\rangle$ therefore increases the desired inversion on the lasing transition between $|1\rangle$ and $|0\rangle$ and hence increses the performance of the laser.

The inversion on the lasing transition can be further improved by replacing the cold bath by a virtual qubit at the virtual temperature

$$T_{\text{vC}} = \frac{\Omega_{\text{C1}} - \Omega_{\text{C2}}}{\Omega_{\text{C1}}/T_{\text{c}} - \Omega_{\text{C2}}/T_{\text{h}}}. \quad (20)$$

Since $T_{\text{h}} > T_{\text{c}}$ and $\Omega_{\text{C2}} = \Omega_{\text{C1}} - (\omega_2 - \omega_1)$, this virtual temperature is always lower than T_{c} .

Hence, the population inversion can be increased for $T_{\text{h}} > (\Omega_{\text{B1}}/\Omega_{\text{B2}})T_{\text{c}}$ if the three-level transitions are not directly coupled to the two thermal baths. This can be seen in Fig. 6 where we plot the population ratio p_1/p_0 as a function of T_{h} .

For the ideal, i.e., lossless, case where the lasing transition is not subject to any additional environment, the optimal population inversion is realised if $T_{\text{vB}} \rightarrow -\infty$ and $T_{\text{vC}} \rightarrow 0$. For fixed bath temperatures, this could, e.g., be achieved by tuning the respective energy spacings Ω_{C1} and Ω_{C2} within the two-qubit machines. However, for the more realistic situation with photon losses through an additional environment at temperature T_{en} that interacts with the lasing transition, the additional coupling Q_{en} competes with the rates to the virtual qubits. Namely, the steady-state of the three-level system explicitly depends on those rates and therefore the optimal virtual temperatures are no longer the same as the ideal lossless case. The reason is as follows; In analogy to Eq. (11), the steady-state of the target qutrit reads

$$\rho_{\text{ss}} \propto (Q_{\text{en}} q_{\text{B}} \tau_{\text{enB}} + q_{\text{B}} q_{\text{C}} \tau_{\text{BC}} + q_{\text{C}} Q_{\text{en}} \tau_{\text{Cen}}). \quad (21)$$

Note that the states $\tau_{\text{enB,BC,Cen}}$ are determined in analogy to Eqs. (12). As seen in Figs. 3 and 4, the rates $q_{\text{B,C}}$ depend on the machine parameters. Therefore, these rates also change while tuning the bath temperatures $T_{\text{h,c}}$ to control the virtual temperatures $T_{\text{vB,vC}}$. By contrast, for the typical heat-pumped three-level laser where the target is directly coupled to the thermal baths, the target relaxes to

$$\rho_{\text{ss}} \propto (Q_{\text{en}} Q_{\text{h}} \tau_{\text{enh}} + Q_{\text{h}} Q_{\text{c}} \tau_{\text{hc}} + Q_{\text{c}} Q_{\text{en}} \tau_{\text{cen}}). \quad (22)$$

To demonstrate that our proposed scheme can still outperform the typical three-level laser even in the non-ideal, lossy, case, we show the dependence of the population ratio p_1/p_0 obtained from Eq. (21) and Eq. (22), respectively, as a function of the hot-bath temperature in Fig. 6. To this end we chose fixed values for the couplings Q_{h} , Q_{c} and Q_{en} and set the effective rates to be

$$q_{\text{B}} = Q_{\text{h}} n_{\text{B}} \quad (23a)$$

$$q_{\text{C}} = Q_{\text{c}} n_{\text{C}}, \quad (23b)$$

with the norms (15) to allow for a fair comparison between the two laser setups in Fig. 5. Namely, we assume the internal details of the two-qubit machines [yellow boxes in Fig. 5(b)] to be tuned in such a way that the effective rates are Eqs. (23). It can be seen from Fig. 6 that using the more complex setup with virtual qubits the population inversion of the lasing transition can be strongly increased. While this holds for all T_{h} in the lossless case, for the chosen parameters this requires $T_{\text{h}} \gtrsim 32$ in the lossy case. Note that since we only tune T_{h} and leave the other parameters, such as the qubit frequencies, invariant, p_1/p_0 is temperature-dependent and remains finite in the lossless case ($T_{\text{v,B}} \rightarrow -\infty$ would require to additionally tune the qubit frequencies).

V. CONCLUSIONS

Designing complex thermal machines at the quantum scale is hard, as they quickly become intractable. We have instead decided to model only the steady state of an arbitrary-dimensional target system in contact with a complex machinery coupled to different heat baths. This can be done by means of competing virtual qubits, coupled to the different transitions of the quantum target. Using reset-type master equations, this enables an analytical solution for all dimensions. We have studied and showcased the behaviour in dimension three, comparing it to full solutions of optical (GKLS) master equations and showed that they share central features and behaviours, whereas the exact target state can at times be different. The models are nonetheless useful for designing machines to optimise certain key properties of the target system, such as inverting the population of the lasing transition in a three-level laser, or generally to optimally create purity in a subspace of the multi-level system.

ACKNOWLEDGMENTS

A.U. acknowledges support from IQOQI-Vienna for visiting, financial support from OIST Graduate University, Research Fellowship of JSPS for Young Scientists, and JSPS KAKENHI Grant Number 20J10006. W.N. acknowledges support from an ESQ fellowship of the Austrian Academy of Sciences (ÖAW). M.H. also acknowledges funds from the FQXi (FQXi-IAF19-03-S2) within the project “*Fueling quantum field machines with information*” and from the Austrian Science Fund (FWF) through the START project Y879-N27. All authors acknowledge productive discussions with the QUIT physics group.

- [1] R. Alicki, The quantum open system as a model of the heat engine, *J. Phys. A* **12**, L103 (1979).
- [2] R. Kosloff, A quantum mechanical open system as a model of a heat engine, *J. Chem. Phys.* **80**, 1625 (1984).
- [3] R. Kosloff, Quantum Thermodynamics: A Dynamical Viewpoint, *Entropy* **15**, 2100 (2013).
- [4] D. Gelbwaser-Klimovsky, W. Niedenzu, and G. Kurizki, Thermodynamics of Quantum Systems Under Dynamical Control, *Adv. At. Mol. Opt. Phys.* **64**, 329 (2015).
- [5] J. Goold, M. Huber, A. Riera, L. del Rio, and P. Skrzypczyk, The role of quantum information in thermodynamics—a topical review, *J. Phys. A* **49**, 143001 (2016).
- [6] S. Vinjanampathy and J. Anders, Quantum thermodynamics, *Contemp. Phys.* **57**, 545 (2016).
- [7] A. Ghosh, W. Niedenzu, V. Mukherjee, and G. Kurizki, Thermodynamic Principles and Implementations of Quantum Machines, in *Thermodynamics in the Quantum Regime*, edited by F. Binder, L. A. Correa, C. Gogolin, J. Anders, and G. Adesso (Springer, Cham, 2019) pp. 37–66.
- [8] S. Bhattacharjee and A. Dutta, Quantum thermal machines and batteries, *arXiv preprint arXiv:2008.07889* (2020).
- [9] J. V. Koski, V. F. Maisi, J. P. Pekola, and D. V. Averin, Experimental realization of a Szilard engine with a single electron, *Proc. Natl. Acad. Sci. USA* **111**, 13786 (2014).
- [10] J. Roßnagel, S. T. Dawkins, K. N. Tolazzi, O. Abah, E. Lutz, F. Schmidt-Kaler, and K. Singer, A single-atom heat engine, *Science* **352**, 325 (2016).
- [11] J. Klaers, S. Faelt, A. Imamoglu, and E. Togan, Squeezed Thermal Reservoirs as a Resource for a Nanomechanical Engine beyond the Carnot Limit, *Phys. Rev. X* **7**, 031044 (2017).
- [12] J. P. S. Peterson, T. B. Batalhão, M. Herrera, A. M. Souza, R. S. Sarthour, I. S. Oliveira, and R. M. Serra, Experimental Characterization of a Spin Quantum Heat Engine, *Phys. Rev. Lett.* **123**, 240601 (2019).
- [13] D. von Lindenfels, O. Gräß, C. T. Schmiegelow, V. Kaushal, J. Schulz, M. T. Mitchison, J. Goold, F. Schmidt-Kaler, and U. G. Poschinger, Spin Heat Engine Coupled to a Harmonic-Oscillator Flywheel, *Phys. Rev. Lett.* **123**, 080602 (2019).
- [14] J. Klatzow, J. N. Becker, P. M. Ledingham, C. Weinzel, K. T. Kaczmarek, D. J. Saunders, J. Nunn, I. A. Walmsley, R. Uzdin, and E. Poem, Experimental Demonstration of Quantum Effects in the Operation of Microscopic Heat Engines, *Phys. Rev. Lett.* **122**, 110601 (2019).
- [15] N. Brunner, N. Linden, S. Popescu, and P. Skrzypczyk, Virtual qubits, virtual temperatures, and the foundations of thermodynamics, *Phys. Rev. E* **85**, 051117 (2012).
- [16] P. Skrzypczyk, N. Brunner, N. Linden, and S. Popescu, The smallest refrigerators can reach maximal efficiency, *J. Phys. A: Math. Theor.* **44**, 492002 (2011).
- [17] N. Linden, S. Popescu, and P. Skrzypczyk, How Small Can Thermal Machines Be? The Smallest Possible Refrigerator, *Phys. Rev. Lett.* **105**, 130401 (2010).
- [18] P. Erker, M. T. Mitchison, R. Silva, M. P. Woods, N. Brunner, and M. Huber, Autonomous Quantum Clocks: Does Thermodynamics Limit Our Ability to Measure Time? *Phys. Rev. X* **7**, 031022 (2017).
- [19] G. Manzano, R. Silva, and J. M. R. Parrondo, Autonomous thermal machine for amplification and control of energetic coherence, *Phys. Rev. E* **99**, 042135 (2019).
- [20] S. Seah, S. Nimmrichter, and V. Scarani, Refrigeration beyond weak internal coupling, *Phys. Rev. E* **98**, 012131 (2018).
- [21] R. Silva, G. Manzano, P. Skrzypczyk, and N. Brunner, Performance of autonomous quantum thermal machines: Hilbert space dimension as a thermodynamical resource, *Phys. Rev. E* **94**, 032120 (2016).
- [22] H. E. D. Scovil and E. O. Schulz-DuBois, Three-Level Masers as Heat Engines, *Phys. Rev. Lett.* **2**, 262 (1959).
- [23] G. Lindblad, On the generators of quantum dynamical semigroups, *Commun. Math. Phys.* **48**, 119 (1976).
- [24] V. Gorini, A. Kossakowski, and E. C. G. Sudarshan, Completely positive dynamical semigroups of N-level systems, *J. Math. Phys.* **17**, 821 (1976).
- [25] H.-P. Breuer and F. Petruccione, *The Theory of Open Quantum Systems* (Oxford University Press, Oxford, 2002).
- [26] A. Tavakoli, G. Haack, M. Huber, N. Brunner, and J. B. Brask, Heralded generation of maximal entanglement in any dimension via incoherent coupling to thermal baths, *Quantum* **2**, 73 (2018).
- [27] S. Krämer, D. Plankensteiner, L. Ostermann, and H. Ritsch, QuantumOptics.jl: A Julia framework for simulating open quantum systems, *Comput. Phys. Commun.* **227**, 109 (2018).
- [28] P. K. Mogensen and A. N. Riseth, Optim: A mathematical optimization package for Julia, *J. Open Source Softw.* **3**, 615 (2018).
- [29] E. Boukobza and D. J. Tannor, Three-Level Systems as Amplifiers and Attenuators: A Thermodynamic Analysis, *Phys. Rev. Lett.* **98**, 240601 (2007).
- [30] W. Niedenzu, M. Huber, and E. Boukobza, Concepts of work in autonomous quantum heat engines, *Quantum* **3**, 195 (2019).

Appendix A: Steady-state solution of effRME for n -level target system

We discuss the steady state for effRME in a multi-level system with some two-qubit machines coupled. For simplicity, let us adhere to cases where every level of the target is coupled to one machine. In these cases, for n -level systems the number of the couplings is $\binom{n}{2} = n(n-1)/2$.

We generalise the effRME to n -level systems. For distinct representation, let us introduce different notation of coupling strength from that in Fig. 2. We write $q_{k,l}$ as the thermalisation rate of the k th and l th levels ($k < l$). The indices A, B, C in Fig. 2 are associated with $q_{0,1}$, $q_{0,2}$, and $q_{1,2}$, respectively. The effRME for n -level target system is written as

$$\frac{\partial \rho}{\partial t} = \sum_{l=1}^{n-1} \sum_{k=0}^{l-1} q_{k,l} (\tau_{k,l} \otimes \text{Tr}_{k,l}[\rho] - \rho), \quad (\text{A1})$$

where $\tau_{k,l}$ is a thermal state at the virtual temperature associated with the k -th and l -th levels and $\text{Tr}_{k,l}$ traces out the space of the k -th and l -th levels. We ignore off-diagonal terms in the density matrix since in this model coherence cannot be generated. Then, this equation can be simplified as

$$\frac{\partial \rho}{\partial t} = \sum_{l=1}^{n-1} \sum_{k=0}^{l-1} q_{k,l} \left(-\tau_{k,l}^e \rho^{(k)} + \tau_{k,l}^g \rho^{(l)} \right) (|k\rangle\langle k| - |l\rangle\langle l|), \quad (\text{A2})$$

with $\rho^{(k)} = \langle k|\rho|k\rangle$. To obtain the steady state, we solve $\partial\rho/\partial t = 0$, i.e.

$$\sum_{l=1}^{n-1} \sum_{k=0}^{l-1} C_{k,l} (|k\rangle\langle k| - |l\rangle\langle l|) = 0, \quad (\text{A3})$$

where $C_{k,l} = q_{k,l} \left(-\tau_{k,l}^e \rho^{(k)} + \tau_{k,l}^g \rho^{(l)} \right)$ and always $k < l$.

First, let us separate the equation into two terms as

$$\sum_{l=1}^{n-1} \sum_{k=0}^{l-1} C_{k,l} |k\rangle\langle k| - \sum_{l=1}^{n-1} \sum_{k=0}^{l-1} C_{k,l} |l\rangle\langle l| = 0. \quad (\text{A4})$$

The first term can be written in a different way,

$$\begin{aligned} \sum_{l=1}^{n-1} \sum_{k=0}^{l-1} C_{k,l} |k\rangle\langle k| &= \sum_{l=1}^{n-1} C_{0,l} |0\rangle\langle 0| + \sum_{l=2}^{n-1} C_{1,l} |1\rangle\langle 1| \\ &\quad + \cdots + \sum_{l=n-1}^{n-1} C_{n-2,l} |n-2\rangle\langle n-2| \\ &= \sum_{s=0}^{n-2} \sum_{l=s+1}^{n-1} C_{s,l} |s\rangle\langle s| \\ &= \sum_{l=1}^{n-1} C_{0,l} |0\rangle\langle 0| + \sum_{s=1}^{n-2} \sum_{l=s+1}^{n-1} C_{s,l} |s\rangle\langle s|, \end{aligned} \quad (\text{A5})$$

and also the second term can be written as

$$\sum_{l=1}^{n-1} \sum_{k=0}^{l-1} C_{k,l} |l\rangle\langle l| = \sum_{l=1}^{n-2} \sum_{k=0}^{l-1} C_{k,l} |l\rangle\langle l| + \sum_{k=0}^{n-2} C_{k,n-1} |n-1\rangle\langle n-1|. \quad (\text{A6})$$

Thus,

$$\begin{aligned} \text{L.H of Eq. (A4)} &= \sum_{l=1}^{n-1} C_{0,l} |0\rangle\langle 0| - \sum_{k=0}^{n-2} C_{k,n-1} |n-1\rangle\langle n-1| \\ &\quad + \sum_{s=1}^{n-2} \sum_{l=s+1}^{n-1} C_{s,l} |s\rangle\langle s| - \sum_{l=1}^{n-2} \sum_{k=0}^{l-1} C_{k,l} |l\rangle\langle l| \\ &= \sum_{l=1}^{n-1} C_{0,l} |0\rangle\langle 0| - \sum_{k=0}^{n-2} C_{k,n-1} |n-1\rangle\langle n-1| \\ &\quad + \sum_{s=1}^{n-2} \left(\sum_{l=s+1}^{n-1} C_{s,l} - \sum_{k=0}^{s-1} C_{k,s} \right) |s\rangle\langle s|. \end{aligned} \quad (\text{A7})$$

Since each of the terms in Eq. (A4) is zero, we can obtain n equations such as

$$\sum_{l=s+1}^{n-1} C_{s,l} - \sum_{k=0}^{s-1} C_{k,s} = 0, \text{ for } \{1 \leq k \leq n-2 : \forall k \in \mathbb{Z}\}, \quad (\text{A8})$$

$$\sum_{l=1}^{n-1} C_{0,l} = 0, \quad (\text{A9})$$

$$\sum_{k=0}^{n-2} C_{k,n-1} = 0. \quad (\text{A10})$$

We arrange a simultaneous equation of the above n equations with a matrix,

$$\tilde{\mathbf{M}}_n \tilde{\rho}_{ss} = \mathbf{0} \quad (\text{A11})$$

where $\tilde{\rho}_{ss} = (\rho_{ss}^{(0)}, \rho_{ss}^{(1)}, \dots, \rho_{ss}^{(n-1)})^T$ and a n -by- n matrix $\tilde{\mathbf{M}}_n$ is given by

$$\tilde{\mathbf{M}} = \begin{pmatrix} M_{0,0} & q_{0,1}\tau_{0,1}^g & q_{0,2}\tau_{0,2}^g & \cdots & q_{0,n-2}\tau_{0,n-2}^g & q_{0,n-1}\tau_{0,n-1}^g \\ q_{0,1}\tau_{0,1}^e & M_{1,1} & q_{1,2}\tau_{1,2}^g & \cdots & q_{1,n-2}\tau_{1,n-2}^g & q_{1,n-1}\tau_{1,n-1}^g \\ q_{0,2}\tau_{0,2}^e & q_{1,2}\tau_{1,2}^e & \ddots & \ddots & \vdots & \vdots \\ \vdots & \vdots & & \ddots & \vdots & \vdots \\ q_{0,n-2}\tau_{0,n-2}^e & q_{1,n-2}\tau_{1,n-2}^e & \cdots & q_{n-3,n-2}\tau_{n-3,n-2}^e & M_{n-2,n-2} & q_{n-2,n-1}\tau_{n-2,n-1}^g \\ q_{0,n-1}\tau_{0,n-1}^e & q_{1,n-1}\tau_{1,n-1}^e & \cdots & q_{n-3,n-1}\tau_{n-3,n-1}^e & q_{n-2,n-1}\tau_{n-2,n-1}^e & M_{n-1,n-1} \end{pmatrix}, \quad (\text{A12})$$

where the diagonal terms are given by $M_{0,0} = -\sum_{s=1}^{n-1} q_{0,s}\tau_{0,s}^e$, $M_{k,k} = -\left(\sum_{s=0}^{k-1} q_{s,k}\tau_{s,k}^g + \sum_{s=k+1}^{n-1} q_{k,s}\tau_{k,s}^e\right)$ for $1 \leq k \leq n-2$, and $M_{n-1,n-1} = -\sum_{s=0}^{n-2} q_{s,n-1}\tau_{s,n-1}^g$. If the inverse matrix of $\tilde{\mathbf{M}}$ exists, we have $\tilde{\rho}_{ss} = 0$: no steady state. Since this is not true physically, we can assume non existence of inverse matrix of $\tilde{\mathbf{M}}$. Here, remem-

ber that the normalisation constraint is not included yet, $\text{Tr}[\rho_{ss}] = 1$. So, we have $(n+1)$ equations even though there are only n elements in $\tilde{\rho}_{ss}$. This indicates that one of the equations is in surplus. We replace the surplus with $\text{Tr}[\rho_{ss}] = 1$. In fact, any row of $\tilde{\mathbf{M}}$ can be removed. For example, the first row can be removed by looking at

the determinant and adding all the rows to the first row,

$$\begin{aligned}
 & \begin{vmatrix} M_{0,0} & q_{0,1}\tau_{0,1}^g & q_{0,2}\tau_{0,2}^g & \cdots & q_{0,n-2}\tau_{0,n-2}^g & q_{0,n-1}\tau_{0,n-1}^g \\ q_{0,1}\tau_{0,1}^e & M_{1,1} & q_{1,2}\tau_{1,2}^g & \cdots & q_{1,n-2}\tau_{1,n-2}^g & q_{1,n-1}\tau_{1,n-1}^g \\ q_{0,2}\tau_{0,2}^e & q_{1,2}\tau_{1,2}^e & \ddots & \ddots & \vdots & \vdots \\ \vdots & \vdots & \ddots & \ddots & \vdots & \vdots \\ q_{0,n-2}\tau_{0,n-2}^e & q_{1,n-2}\tau_{1,n-2}^e & \cdots & q_{n-3,n-2}\tau_{n-3,n-2}^e & M_{n-2,n-2} & q_{n-2,n-1}\tau_{n-2,n-1}^g \\ q_{0,n-1}\tau_{0,n-1}^e & q_{1,n-1}\tau_{1,n-1}^e & \cdots & q_{n-3,n-1}\tau_{n-3,n-1}^e & q_{n-2,n-1}\tau_{n-2,n-1}^e & M_{n-1,n-1} \end{vmatrix} \\
 = & \begin{vmatrix} 0 & 0 & 0 & \cdots & 0 & 0 \\ q_{0,1}\tau_{0,1}^e & M_{1,1} & q_{1,2}\tau_{1,2}^g & \cdots & q_{1,n-2}\tau_{1,n-2}^g & q_{1,n-1}\tau_{1,n-1}^g \\ q_{0,2}\tau_{0,2}^e & q_{1,2}\tau_{1,2}^e & \ddots & \ddots & \vdots & \vdots \\ \vdots & \vdots & \ddots & \ddots & \vdots & \vdots \\ q_{0,n-2}\tau_{0,n-2}^e & q_{1,n-2}\tau_{1,n-2}^e & \cdots & q_{n-3,n-2}\tau_{n-3,n-2}^e & M_{n-2,n-2} & q_{n-2,n-1}\tau_{n-2,n-1}^g \\ q_{0,n-1}\tau_{0,n-1}^e & q_{1,n-1}\tau_{1,n-1}^e & \cdots & q_{n-3,n-1}\tau_{n-3,n-1}^e & q_{n-2,n-1}\tau_{n-2,n-1}^e & M_{n-1,n-1} \end{vmatrix}. \quad (A13)
 \end{aligned}$$

We replace the first row with $\text{Tr}[\rho_{ss}] = 1$, and the simultaneous equation (A11) changes to

$$\mathbf{M} \begin{pmatrix} \rho_{ss}^{(0)} \\ \rho_{ss}^{(1)} \\ \vdots \\ \rho_{ss}^{(n-1)} \end{pmatrix} = \begin{pmatrix} 1 \\ 0 \\ \vdots \\ 0 \end{pmatrix}, \quad (A14)$$

where the matrix \mathbf{M} is defined as

$$\mathbf{M} = \begin{pmatrix} 1 & 1 & 1 & \cdots & 1 & 1 \\ q_{0,1}\tau_{0,1}^e & M_{1,1} & q_{1,2}\tau_{1,2}^g & \cdots & q_{1,n-2}\tau_{1,n-2}^g & q_{1,n-1}\tau_{1,n-1}^g \\ q_{0,2}\tau_{0,2}^e & q_{1,2}\tau_{1,2}^e & \ddots & \ddots & \vdots & \vdots \\ \vdots & \vdots & \ddots & \ddots & \vdots & \vdots \\ q_{0,n-2}\tau_{0,n-2}^e & q_{1,n-2}\tau_{1,n-2}^e & \cdots & q_{n-3,n-2}\tau_{n-3,n-2}^e & M_{n-2,n-2} & q_{n-2,n-1}\tau_{n-2,n-1}^g \\ q_{0,n-1}\tau_{0,n-1}^e & q_{1,n-1}\tau_{1,n-1}^e & \cdots & q_{n-3,n-1}\tau_{n-3,n-1}^e & q_{n-2,n-1}\tau_{n-2,n-1}^e & M_{n-1,n-1} \end{pmatrix}. \quad (A15)$$

Assuming that the matrix \mathbf{M} is invertible, the solution $\tilde{\rho}_{ss}$ is obtained as

$$\tilde{\rho}_{ss} = \mathbf{M}^{-1} \begin{pmatrix} 1 \\ 0 \\ \vdots \\ 0 \end{pmatrix}. \quad (A16)$$

According to Cramer's rule, the inverse matrix is written as

$$\mathbf{M}^{-1} = \frac{1}{\det[\mathbf{M}]} \text{adj}[\mathbf{M}], \quad (A17)$$

where $\text{adj}[\mathbf{M}]$ is the adjugate of \mathbf{M} , given by $\text{adj}[\mathbf{M}] = [\{\Delta_{i,j}\}_{1 \leq i,j \leq n}]^T$, i.e.

$$\text{adj}[\mathbf{M}] = \begin{pmatrix} \Delta_{1,1} & \Delta_{2,1} & \cdots & \Delta_{n,1} \\ \Delta_{1,2} & \Delta_{2,2} & \cdots & \Delta_{n,2} \\ \vdots & \vdots & \ddots & \vdots \\ \Delta_{1,n} & \Delta_{2,n} & \cdots & \Delta_{n,n} \end{pmatrix}, \quad (A18)$$

where $\Delta_{i,j}$ is a set of the cofactors of the matrix \mathbf{M} and defined as

$$\Delta_{i,j} = (-1)^{i+j} \begin{vmatrix} M_{0,0} & \cdots & M_{0,j-1} & M_{0,j+1} & \cdots & M_{0,n-1} \\ \vdots & \vdots & \vdots & \vdots & \vdots & \vdots \\ M_{i-1,0} & \cdots & M_{i-1,j-1} & M_{i-1,j+1} & \cdots & M_{i-1,n-1} \\ M_{i+1,0} & \cdots & M_{i+1,j-1} & M_{i+1,j+1} & \cdots & M_{i+1,n-1} \\ \vdots & \vdots & \vdots & \vdots & \vdots & \vdots \\ M_{n-1,0} & \cdots & M_{n-1,j-1} & M_{n-1,j+1} & \cdots & M_{n-1,n-1} \end{vmatrix}. \quad (A19)$$

Also, due to the mathematical properties of determinant, $\det[\mathbf{M}] = \sum_{s=1}^n \Delta_{1,s}$. As a results, the solution $\tilde{\rho}_{ss}$ is written as

$$\tilde{\rho}_{ss} = \frac{1}{\sum_{s=1}^n \Delta_{1,s}} \begin{pmatrix} \Delta_{1,1} \\ \Delta_{1,2} \\ \vdots \\ \Delta_{1,n} \end{pmatrix}, \quad (A20)$$

which is normalised as $\sum_{j=1}^n \rho_{ss}^{(j)} = 1$ with $\rho^{(j)}$ being an element of the density matrix. For $n = 2$, the solution (A20) gives the thermal state of the virtual temperature, $\rho_{ss} = (\tau_{0,1}^g, \tau_{0,1}^e)^T$, which is fair. For $n = 3$, the solution (A20) corresponds to Eq. (11). See the Appendix B for the solution for $n = 4$.

Note that we assume of the matrix \mathbf{M} being invertible, and there if there is no inverse matrix for the matrix \mathbf{M} , the steady state cannot be defined. For example, in a case that only one machine is coupled to a four-level system, the population at four of all the levels is not determined.

Appendix B: Steady-state solution of effRME for four-level system

One can obtain the steady state of effRME for any-level target system from Eq. (A20). In this appendix, we focus on a four-level target system and discuss components of its steady state. Let us recall that the steady state (11) of effRME for qutrit target systems is combination of another steady states where two pairs of levels are characterised with different temperatures, weighted with the effective thermalisation rates q_i . Even for higher-level systems, the same feature can be seen. Let us see a four-level target system where each pair of levels are occupied by one two-qubit machine and in total six machines are involved. The steady state of the effRME is given by

$$\begin{aligned} \frac{\rho_{ss}}{C} = & q_0^3 q_1^3 q_2^3 \tau_{012}^{333} \\ & + q_0^3 q_1^3 q_0^2 \tau_{010}^{332} + q_0^3 q_1^3 q_1^2 \tau_{011}^{332} \\ & + q_0^3 q_2^3 q_0^1 \tau_{020}^{331} + q_0^3 q_2^3 q_1^2 \tau_{021}^{332} \\ & + q_1^3 q_2^3 q_0^1 \tau_{120}^{331} + q_1^3 q_2^3 q_0^2 \tau_{120}^{332} \\ & + q_0^3 q_0^1 q_0^2 \tau_{000}^{312} + q_0^3 q_0^1 q_1^2 \tau_{001}^{312} + q_0^3 q_0^2 q_1^2 \tau_{001}^{322} \\ & + q_1^3 q_0^1 q_0^2 \tau_{100}^{312} + q_1^3 q_0^1 q_1^2 \tau_{101}^{312} + q_1^3 q_0^2 q_1^2 \tau_{101}^{322} \\ & + q_2^3 q_0^1 q_0^2 \tau_{200}^{312} + q_2^3 q_0^1 q_1^2 \tau_{201}^{312} + q_2^3 q_0^2 q_1^2 \tau_{201}^{322}, \quad (B1) \end{aligned}$$

where the normalisation is $C = \text{Tr}[\text{R.H. of (B1)}]^{-1}$, and 16 states such as τ_{012}^{333} are steady states with three of the coherent couplings on. For example,

$$\begin{aligned} \tau_{012}^{333} = & \tau_{0,3}^g \tau_{1,3}^e \tau_{2,3}^e |0\rangle\langle 0| + \tau_{0,3}^e \tau_{1,3}^g \tau_{2,3}^e |1\rangle\langle 1| \\ & + \tau_{0,3}^e \tau_{1,3}^e \tau_{2,3}^g |2\rangle\langle 2| + \tau_{0,3}^e \tau_{1,3}^e \tau_{2,3}^e |3\rangle\langle 3|, \quad (B2) \end{aligned}$$

which is not normalised such as Eq. (12) on purpose and where three pairs of the levels are characterised with different temperatures.

Note that the effective steady state (B1) consists of 16 of the steady states where three of the coherent couplings are present in the system (e.g. τ_{012}^{333}). However, also notice that the state (B1) does not cover all the possible steady states with three of the couplings on. The total number of all the possible steady states corresponds to the number of all the combination to choose three couplings from six machines, which is $\binom{6}{3} = 20$. Thus, four

cases are missing in the state (B1). For example, a case is excluded that three two-qubit machines are coupled to the levels between $|0\rangle$ and $|1\rangle$, those between $|0\rangle$ and $|3\rangle$, and those between $|1\rangle$ and $|3\rangle$.

There are some differences between the excluded cases and the included cases. In the excluded cases, one level is unoccupied. For the above example, the level $|2\rangle$ is free. Moreover, the excluded cases are essentially the same as the situation depicted in Fig. 2, i.e. the three thermalisation processes compete.

As discussed in Sec. III.1, this kind of steady state cannot be described simply with just the virtual temperature but the effective rates are required, in contrast to Eq. (B2). In summary, the steady state (B1) is composed of steady states that are not involved with competition against other thermal machines.